Diagn Interv Radiol 2016; 22:201–206
© Turkish Society of Radiology 2016

ABDOMINAL IMAGING
ORIGINAL ARTICLE

Semi-automatic 3D-volumetry of liver metastases from neuroendocrine tumors to improve combination therapy with ^{177}Lu-DOTATOC and ^{90}Y-DOTATOC

Matthaeus Cieciera
Clemens Kratochwil
Jan Moltz
Hans-Ulrich Kauczor
Tim Holland-Letz
Peter Choyke
Walter Mier
Uwe Haberkorn
Frederik L. Giesel

PURPOSE
Patients with neuroendocrine tumors (NET) often present with disseminated liver metastases and can be treated with a number of different nuclides or nuclide combinations in peptide receptor radionuclide therapy (PRRT) depending on tumor load and lesion diameter. For quantification of disseminated liver lesions, semi-automatic lesion detection is helpful to determine tumor burden and tumor diameter in a time efficient manner. Here, we aimed to evaluate semi-automated measurement of total metastatic burden for therapy stratification.

METHODS
Nineteen patients with liver metastasized NET underwent contrast-enhanced 1.5 T MRI using gadolinium-ethoxybenzyl diethylenetriaminepentaacetic acid. Liver metastases (n=1537) were segmented using Fraunhofer MEVIS Software for three-dimensional (3D) segmentation. All lesions were stratified according to longest 3D diameter >20 mm or ≤20 mm and relative contribution to tumor load was used for therapy stratification.

RESULTS
Mean count of lesions ≤20 mm was 67.5 and mean count of lesions >20 mm was 13.4. However, mean contribution to total tumor volume of lesions ≤20 mm was 24%, while contribution of lesions >20 mm was 76%.

CONCLUSION
Semi-automatic lesion analysis provides useful information about lesion distribution in predominantly liver metastasized NET patients prior to PRRT. As conventional manual lesion measurements are laborious, our study shows this new approach is more efficient and less operator-dependent and may prove to be useful in the decision making process selecting the best combination PRRT in each patient.

Neuroendocrine tumors (NETs) are unusual tumors with an incidence of 4 or 5 per 100.000 per year, rising in the past decades, but still representing only about 1% of all malignant neoplasms (1). NETs are often detected when the disease is advanced, commonly presenting with a large number of liver metastases. In addition to surgical resection, focal treatments include selective internal radiation therapy, transarterial chemoembolization, or radiofrequency ablation (2). Due to the large burden of disease, portal vein thrombosis, or hepatic insufficiency, these methods have limitations (3). Thus, there has been increasing interest in palliative treatments with ^{90}Yttrium- (^{90}Y-) DOTA(0)-Phe(1)-Tyr(3)-octreotid (DOTATOC) or ^{177}Lutetium- (^{177}Lu-) DOTATOC which provide response rates of about 30% (4, 5). ^{90}Yttrium and ^{177}Lutetium have different ranges of effective dose distribution with a maximal tissue penetration range of 12 mm (^{90}Y) and 2 mm (^{177}Lu), respectively (6). Thus, therapy regimens might benefit from an adjustment according to lesion size distribution in a given patient, i.e., using ^{90}Y primarily for targeting lesions >20 mm and ^{177}Lu primarily for lesions ≤20 mm in diameter. However, total lesion quantification is time consuming and operator-dependent, resulting in an approximation of total lesion distribution only. Moreover, it can be difficult to manually determine the maximum three-dimensional (3D) diameter. Thus, in patients with a large number of metastases, it can be very challenging to manually quantify the volume of multiple hepatic lesions (7).

Besides ^{68}Ga-DOTATOC positron-emission-tomography/computed tomography (PET/CT) scans for functional imaging, which were recently proven to be capable of predicting thera-

From the Departments of Nuclear Medicine (M.C., C.K., W.M., U.H., F.L.G. ✉ *f.giesel@dkfz-heidelberg.de*) and Radiology (H.U.K.) University Hospital Heidelberg, Heidelberg, Germany; the Institute for Medical Imaging Computing (J.M.), Fraunhofer MEVIS, Bremen; the Department of Biostatistics (T.H.L.), German Cancer Research Center, Germany; the Molecular Imaging Program (P.C.), National Cancer Institute, National Institutes of Health, Bethesda, MD, USA; Clinical Cooperation Unit Nuclear Medicine (U.H., F.L.G.), DKFZ Heidelberg, Germany.

Received 15 July 2015; revision requested 22 August 2015; revision received 25 August 2015; accepted 27 September 2015.

Published online 22 March 2016.
DOI 10.5152/dir.2015.15304

py response in liver lesions (8), contrast-enhanced magnetic resonance imaging (MRI) is the modality of choice for structural assessment (9).

Here, we aimed to evaluate the feasibility of a semi-automated measurement tool designed to determine the total lesion size distribution in patients with metastatic NET. This information can then be used to determine the optimal combination of peptide receptor radionuclide therapy (PRRT) in each patient.

Methods

Patients

We performed this retrospective analysis using the data of 19 consecutive patients (9 males and 10 females; mean age, 53.6 years; age range, 40–69 years) who had a prior histologic diagnosis of NET with confirmed metastases to the liver and underwent PRRT in our institution from June 2009 to May 2011. Some patients had resection of the respective primary tumor, splenectomy, chemotherapies, focal treatments, or therapies using somatostatin analogs, before PRRT. Primary tumors were pancreatic tumor (n=9), intestinal tumor (n=6), lung tumor (n=1), renal tumor (n=1), and neuroendocrine tumor with an unknown primary (n=2). The liver lesions were confirmed to have originated from their respective neuroendocrine tumors using a ^{68}Ga-DOTATOC-PET/CT within 4–6 weeks of study entry. Formal consent was obtained from all participating patients. Ethics committee of our institution approved this study.

Main points

- Patients with liver lesions from neuroendocrine tumors (NET) often present with disseminated liver involvement.
- Patient-individualized ^{177}Lu- and ^{90}Y-DOTATOC nuclide combination could improve peptide receptor radionuclide therapy of NET liver lesions due to their different radiation range and distribution.
- Manual measurements are laborious, and choice of nuclide combination is operator dependent as patients often show numerous liver lesions.
- We describe a new method for semi-automatic liver lesion segmentation, which allows accurate definition of lesion load and distribution based on contrast-enhanced MRI.
- Lesion distribution can be used for dosimetry and therapy stratification.

MRI and PET/CT

All patients underwent hepatic MRI. MRI was performed on a 1.5 T whole body system (Avanto, Siemens) using gadolinium-ethoxybenzyl diethylenetriaminepentaacetic acid (Gd-EOB-DTPA), a hepatocyte specific contrast agent (Primovist, Bayer-Schering). Contrast-enhanced MRI was performed using volumetric interpolated breath-hold examination, which is a T1-weighted scan (TR 3.41 ms, TE 1.18 ms, slice-thickness 4 mm, matrix 320×180; 72 axial slices with an acquisition time of 20 s per 3D dataset). Adjusted to patient weight (0.1 mL/kg), up to 20 mL of 0.25 mol/L contrast was injected at 3 mL/s, followed by injection of 30 mL saline at the same rate. Among other sequences, a hepatocyte phase was acquired 15 minutes after administration and used for this study.

Radiopharmaceuticals

DOTATOC was synthesized as described in the literature (10). ^{68}Ga (half-life, 68.3 min) was obtained from a ^{68}Ge/^{68}Ga radionuclide generator developed by the Radiochemistry Department of the German Research Center in Heidelberg. Twenty-four micrograms of peptide (16.8 nmol of aqueous DOTATOC solution) were used per synthesis. HPLC revealed <2% of unchelated ^{68}Ga. Pyrogenicity and sterility were also evaluated.

^{68}Ga DOTATOC-PET/CT was performed on a Biograph 6 (Siemens/CTI). Imaging was initiated 45±5 min after intravenous injection of 90–198 MBq ^{68}Ga-DOTATOC. Static emission scans, corrected for dead time, scatter and decay, were acquired from the vertex to the proximal legs using eight bed positions at 4 min each. The PET images were iteratively reconstructed with the ordered subset expectation maximization algorithm using four iterations with eight subsets and Gaussian filtering to achieve an in-plane spatial resolution of 5 mm at full-width half-maximum. A low dose CT without contrast agent was obtained for attenuation correction. Contrast-enhanced CT was additionally performed at the time of the PET/CT. PET and MRI were co-registered using Syngo® 3D (Siemens). All images were electronically stored in a picture archiving and communication system.

Image analysis and statistics

Oncology prototype software (Version 1.9.0; 2012-11-15 Release; Qt Version 4.8.0 Fraunhofer MEVIS, Siemens) was used for semi-automated 3D segmentation of liver lesions (11). There is no general consent on a gold standard for volumetric lesion quantification in the presented scenario yet. However, the Fraunhofer method/algorithm has been tested and shown to be reliable (11). In each patient, the Gd-EOB-DTPA MRI dataset underwent volumetric analysis of all identifiable lesions in a semi-automated manner as shown in Figs. 1 and 2. The user sets a seed point in each lesion and the software then automatically delineates the lesion's edges. Each segmentation was checked by the user in every frame of the dataset in three axes and corrected if necessary. After calculation of the volume and maximal 3D diameter in mm, each lesion was assigned to one of two groups (Group 1 ≤20 mm in longest 3D diameter, Group 2 >20 mm in longest 3D diameter). After this, lesion volume distribution was analyzed by adding up the volumes of all lesions in each

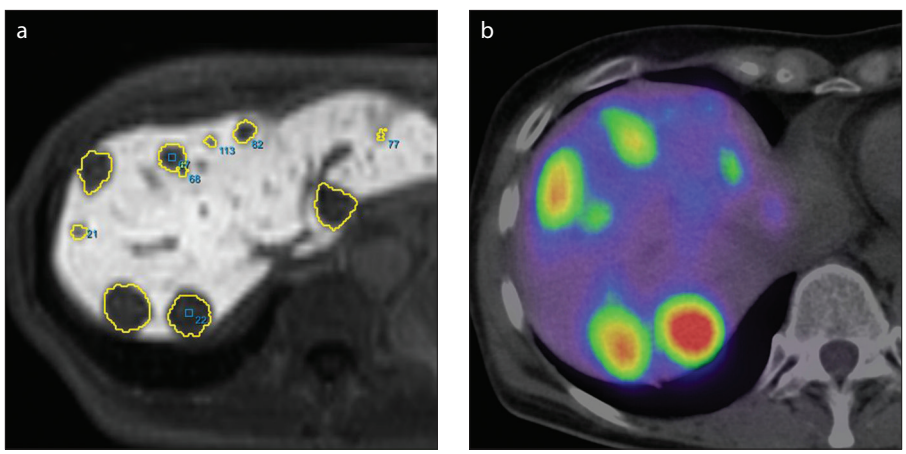

Figure 1. a, b. Images depicting examples of lesion mapping for lesion distribution analysis and peptide receptor radionuclide therapy stratification. Lesions from Gd-EOB-DTPA MRI **(a)** were compared with a DOTATOC-PET/CT scan **(b)** to validate their origin. The images originate from patient 13.

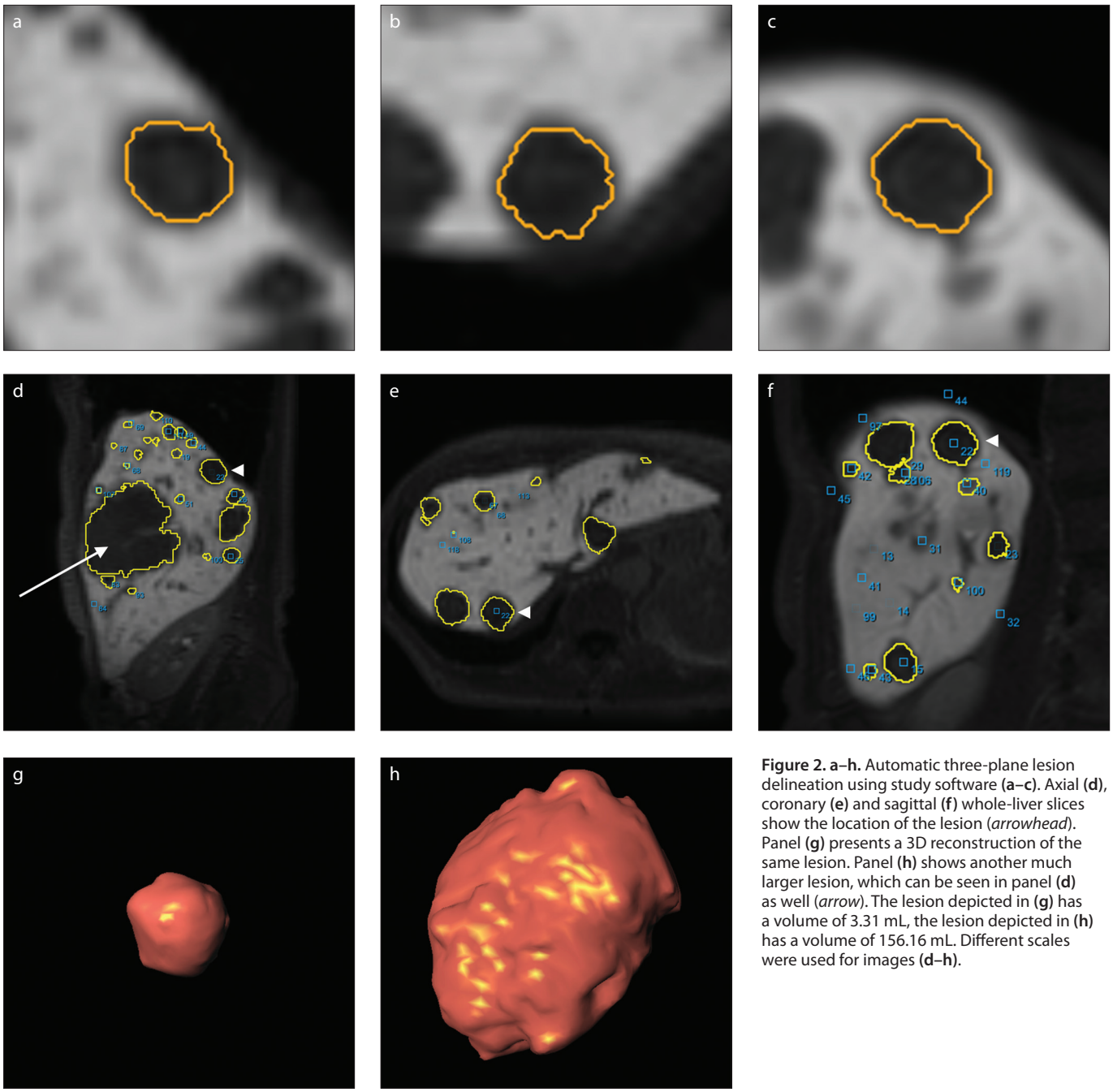

Figure 2. a–h. Automatic three-plane lesion delineation using study software **(a–c)**. Axial **(d)**, coronary **(e)** and sagittal **(f)** whole-liver slices show the location of the lesion (*arrowhead*). Panel **(g)** presents a 3D reconstruction of the same lesion. Panel **(h)** shows another much larger lesion, which can be seen in panel **(d)** as well (*arrow*). The lesion depicted in **(g)** has a volume of 3.31 mL, the lesion depicted in **(h)** has a volume of 156.16 mL. Different scales were used for images **(d–h)**.

of the two respective groups and dividing this value by the total tumor volume in each patient. Total tumor load was defined as the sum of all lesion volumes in a patient. This provided the percentage volume of large vs. small tumors in each patient.

Results

Lesion measurements were successfully quantified in all lesions of all patients; a total of 1537 lesions were quantified. The tumor burden of the patients assessed ranged from 5 mL to 788 mL.

The mean count of lesions ≤20 mm was 67 per patient (standard deviation [SD], 87; range, 0–351), while the mean count of lesions >20 mm was 13 per patient (SD, 14; range, 0–50). However, the mean contribution of lesions ≤20 mm to tumor volume was only 24% (SD, 24%; range, 0%–100%), while the contribution of lesions >20 mm was 76% (SD, 24%; range, 0%–100%). The mean maximal 3D diameter (mean of all patient's means) was 16.6 mm (SD, 5.5 mm; range, 10.2–31.7 mm). The mean individual tumor volume (mean of all patient's means) was 5 mL (SD, 7 mL; range, 0.36–31 mL).

Fig. 3 shows two connected columns for each patient who presented with one or more liver lesions that were ≤20 mm (patient 16 had lesions >20 mm only). The relation of share of lesion count to share of total tumor load of the participating patients presented as follows: mean, 8.995; SD, 15.569; range, 0.000–60.896; median, 3.484.

For a more detailed analysis of a patient's tumor load, a chart was prepared for every patient individually. The charts depict distribution of the volumes and counts of all lesions, ordered according to their size and categorized in size-groups according

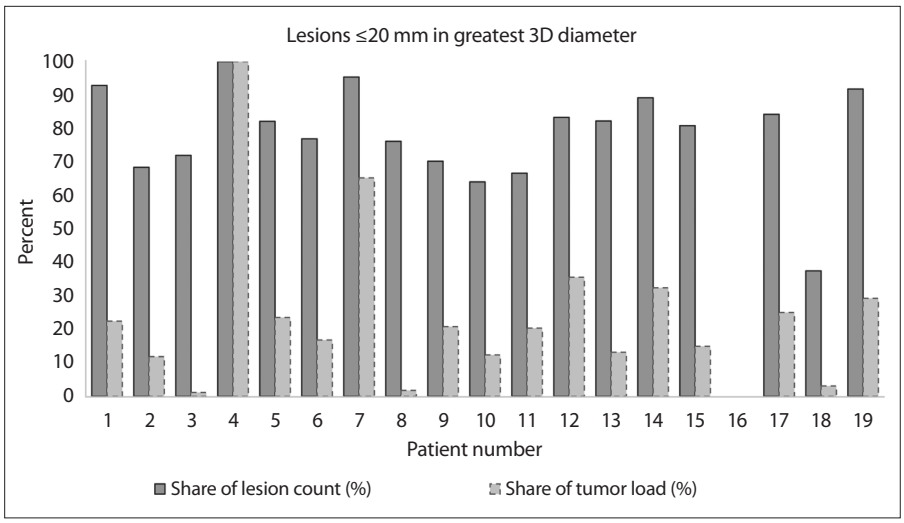

Figure 3. Lesions ≤20 mm in greatest 3D diameter; individual comparison of share of total lesion count with share of total tumor load in each patient. The darker column represents the percentage of the total lesion count contributed by lesions ≤20 mm; e.g., in patient 1, 52 of 56 lesions were ≤20 mm in maximal diameter thus showing as 93%. The lighter column represents each patient's corresponding percentage of total tumor load contributed by lesions ≤20 mm; e.g., in the same patient 1, of the 60 mL total tumor load, 14 mL were from lesions ≤20 mm, thus showing as 23%. Note that there is a clear difference between the two values in most patients.

to their maximal 3D-diameter, using 1 mm steps for each new group. In each of these groups, the volumes of the lesions in the group were added to calculate the size-group's total volume in mL. Two of these charts are shown in Fig. 4, representing patient 13 (Fig. 4a) and patient 7 (Fig. 4b).

Discussion

In our study, the tumor load of all participating patients has successfully been evaluated, with a total of 1537 assessed liver lesions. Semi-automatic volumetric lesion analysis is a feasible approach, which can help determine a user-independent, patient-specific combination PRRT. Combination PRRT employing both ^{177}Lu-DOTATOC and ^{90}Y-DOTATOC has been shown to be a superior therapy to either method alone in patients with metastatic NETs to the liver (12). However, accurate depiction of lesion spread is important to perform PRRT properly. Using Gd-EOB-DTPA, an intravenous contrast agent that binds hepatocytes, the margins of the hepatic metastases become highly visible enabling the accurate determination of lesion size and distribution of lesion volume. The most appropriate mix of ^{177}Lu-DOTATOC (2 mm range) and ^{90}Y-DOTATOC (12 mm range) could then be selected. However, manual determination of each lesion is labor-intensive in patients with one hundred or more lesions and are additionally subject to observer error. Therefore, a robust, software-assisted method of determining the volume contribution of different size lesions would be useful.

Calculation of the contribution to total tumor volume from smaller and larger lesions is the ultimate goal of this software. Currently, the software is able to quickly segment and determine the volume and maximum diameter in 3D of identified liver metastases. However, the final calculations must still be done in a spreadsheet. Eventually, this step will be integrated into the software so that the output is automatic. Also, fully automated lesion detection and liver segmentation would significantly shorten the time needed to assess a patient. If a fully automated system is developed, it becomes more feasible to introduce a third category of lesion size based on yet another radioisotope, ^{213}Bismuth (^{213}Bi, 75 µm range) to further customize treatments for each patient (13).

Fig. 5 shows idealized lesion size distribution curves on which to base radioisotope selection in an individual patient. These curves represent abstracted forms of the volume distribution shown in Fig. 4. For patients with predominantly large lesions monotherapy with ^{90}Y-DOTATOC will produce the best results for the available dose. For patients with a mixture of larger and moderate size lesions, a combination of ^{90}Y-DOTATOC and ^{177}Lu-DOTATOC will be more successful. For patients with mixtures of small and moderate size lesions a combination of ^{177}Lu-DOTATOC and ^{213}Bi-DOTATOC is preferred. Using dosimetry data, it is possible to determine the exact contribution of each radionuclide based on the geometry and distribution of the lesions. The acquisition and utilization of the data necessary for this is a computationally intensive approach, which is possible only by accurately characterizing the location, size, and volume of each lesion in relationship to each other, thus, by accurately describing the total tumor load of a patient. Although this is the ultimate goal of our study, there is still much work to be done in mathematical modeling of the radiation dose and predicting appropriate mixtures of radioisotopes. Therapy schemes may be further complicated by knowledge of previous efficacy and tolerability of PRRT. However, none of this is possible without first accurately categorizing the extent of disease.

This study has a number of limitations. There is still a certain degree of operator-dependency, as the actual lesion delineation was performed manually. Differences among users might also contribute to errors. The reliability of semi-automatic volumetric analysis is subject to ongoing research. Studies comparing the interobserver and/or intraobserver variability between semi-automatic and manual volume measurements have shown comparable results, namely, a superiority of semi-automatic measurements, depending on entity and used modality (14–17). Also, this method depends on detection of lesions following Gd-EOB-DTPA enhancement. Although most lesions can be distinguished against the liver, undoubtedly there are lesions that do not contrast sufficiently to enable accurate identification and segmentation. Thus, patients with highly disseminated metastases of the liver and patients who present with advanced stage hepatic fibrosis or scarring may not be good candidates for this method. Furthermore, the error rate of the semi-automated delineation was not assessed. It is still unknown whether a more accurate depiction of lesion size will result in clinically significant differences in the outcomes of patients undergoing PRRT. Evidence of its possible superiority can only be proven by a controlled, double-blind randomized study, which will likely require many patients. A 1.5T MRI was used for this study as it was available in our institution. Using a 3T MRI might enhance accuracy of lesion assessment, especially in smaller lesions.

In conclusion, we demonstrated that a segmentation software is capable of help-

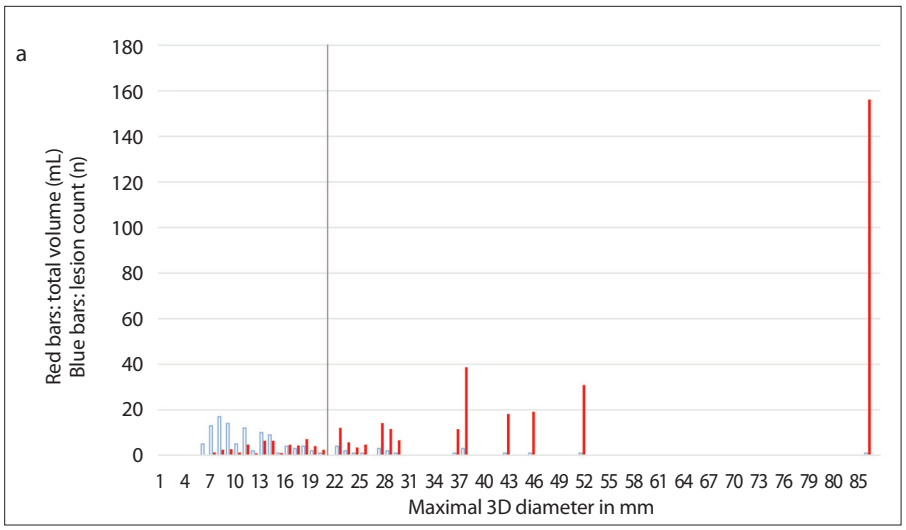

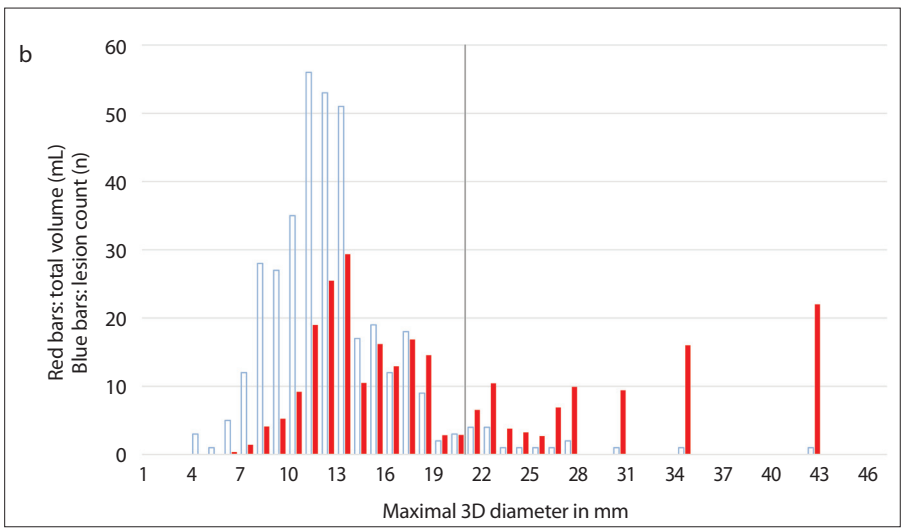

Figure 4 . a, b. Analysis of tumor load; red bars indicate the size-group's total volume in mL, blue bars indicate the lesion count. Chart **(a)** shows the tumor load distribution of patient 13 with a total of 144 lesions, 102 of them ≤20 mm. Yet these lesions contribute to only 13.2% of the total tumor load. In comparison, chart **(b)** shows patient 7 with a total of 368 lesions, 351 of them ≤20 mm. These lesions contribute to 65.3% of the total tumor load. Note the cutoff lines at 20 mm. The total volumes of the groups are depicted in the charts as red/filled bars beginning with the smallest group to the left and the largest group to the right; e.g., in chart **(b)**, the 10 mm group had a total added volume of 9 mL. The blue/empty bars represent the same size-groups, but depict the number of lesions that make each group up; e.g., in chart **(b)**, the 10 mm group consists of 35 lesions.

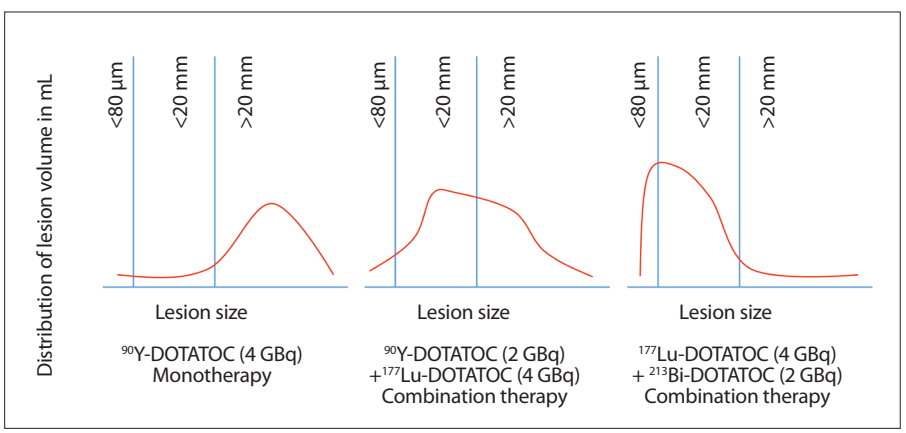

Figure 5. Idealized therapy stratification based on lesion distribution curves using segmentation of Gd-EOB-DTPA MRI.

ing users quantify the volume and maximum diameter of all hepatic metastases in patients with NET. This might enable user independent PRRT stratification. Current manual methods of lesion characterization are time consuming and inaccurate and thus semi-automated and fully automated methods described here will greatly improve the ability to perform dosimetry and combination PRRT. Although the segmentation process is yet to be optimized, it is clear that this method provides faster and more reliable lesion mapping, volume, and maximum 3D diameters than what is currently possible.

Conflict of interest disclosure

The authors declared no conflicts of interest.

References

1. Yao JC, Hassan M, Phan A, et al. One hundred years after "carcinoid": epidemiology of and prognostic factors for neuroendocrine tumors in 35,825 cases in the United States. J Clin Oncol 2008; 26:3063–3072. [CrossRef]
2. Del Prete M, Fiore F, Modica R, et al. Hepatic arterial embolization in patients with neuroendocrine tumors. J Exp Clin Cancer Res 2014; 33:43. [CrossRef]
3. Kratochwil C, Giesel FL, Lopez-Benitez R, et al. Intraindividual comparison of selective arterial versus venous 68Ga-DOTATOC PET/CT in patients with gastroenteropancreatic neuroendocrine tumors. Clin Cancer Res 2010; 16:2899–2905. [CrossRef]
4. Bodei L, Pepe G, Paganelli G. Peptide receptor radionuclide therapy (PRRT) of neuroendocrine tumors with somatostatin analogues. Eur Rev Med Pharmacol Sci 2010; 14:347–351.
5. Kwekkeboom DJ, de Herder WW, Kam BL, et al. Treatment with the radiolabeled somatostatin analog [177 Lu-DOTA 0,Tyr3]octreotate: toxicity, efficacy, and survival. J Clin Oncol 2008; 26:2124–2130. [CrossRef]
6. Van Essen M, Krenning EP, De Jong M, Valkema R, Kwekkeboom DJ. Peptide receptor radionuclide therapy with radiolabelled somatostatin analogues in patients with somatostatin receptor positive tumours. Acta Oncol 2007; 46:723–734. [CrossRef]
7. de Jong M, Breeman WA, Valkema R, Bernard BF, Krenning EP. Combination radionuclide therapy using 177Lu- and 90Y-labeled somatostatin analogs. J Nucl Med 2005; 46 (Suppl 1):13S–17S.
8. Kratochwil C, Stefanova M, Mavriopoulou E, et al. SUV of [Ga]DOTATOC-PET/CT predicts response probability of PRRT in neuroendocrine tumors. Mol Imaging Biol 2015; 17:313–318. [CrossRef]
9. Giesel FL, Kratochwil C, Mehndiratta A, et al. Comparison of neuroendocrine tumor detection and characterization using DOTATOC-PET in correlation with contrast-enhanced CT and delayed contrast-enhanced MRI. Eur J Radiol 2012; 81:2820–2825. [CrossRef]

10. Otte A, Mueller-Brand J, Dellas S, Nitzsche EU, Herrmann R, Maecke HR. Yttrium-90-labelled somatostatin-analogue for cancer treatment. Lancet 1998; 351:417–418. [CrossRef]
11. Moltz JH, Bornemann L, Kuhnigk JM, et al. Advanced segmentation techniques for lung nodules, liver metastases, and enlarged lymph nodes in CT scans. IEEE J Sel Top Signal Process 2009; 3:122–134. [CrossRef]
12. Villard L, Romer A, Marincek N, et al. Cohort study of somatostatin-based radiopeptide therapy with [(90)Y-DOTA]-TOC versus [(90)Y-DOTA]-TOC plus [(177)Lu-DOTA]-TOC in neuroendocrine cancers. J Clin Oncol 2012; 30:1100–1106. [CrossRef]
13. Giesel FL, Wulfert S, Zechmann CM, et al. Contrast-enhanced ultrasound monitoring of perfusion changes in hepatic neuroendocrine metastases after systemic versus selective arterial 177Lu/90Y-DOTATOC and 213Bi-DOTATOC radiopeptide therapy. Exp Oncol 2013; 35:122–126.
14. Dinkel J, Khalilzadeh O, Hintze C, et al. Inter-observer reproducibility of semi-automatic tumor diameter measurement and volumetric analysis in patients with lung cancer. Lung Cancer 2013; 82:76–82. [CrossRef]
15. Rexilius J, Hahn HK, Schluter M, Bourquain H, Peitgen HO. Evaluation of accuracy in MS lesion volumetry using realistic lesion phantoms. Acad Radiol 2005; 12:17–24. [CrossRef]
16. Wulff AM, Bolte H, Fischer S, et al. Lung, liver and lymph node metastases in follow-up MSCT: comprehensive volumetric assessment of lesion size changes. Rofo 2012; 184:820–828. [CrossRef]
17. van Kessel CS, van Leeuwen MS, Witteveen PO, Kwee TC, Verkooijen HM, van Hillegersberg R. Semi-automatic software increases CT measurement accuracy but not response classification of colorectal liver metastases after chemotherapy. Eur J Radiol 2012; 81:2543–2549. [CrossRef]